



HAL
open science

Origin of Pr 3+ luminescence in hafnium silicate films: combined atom probe tomography and TEM investigations

Rémi Demoulin, Georges Beainy, Celia Castro, Philippe Pareige, Larysa Khomenkova, Christophe Labbé, Fabrice Gourbilleau, Etienne Talbot

► To cite this version:

Rémi Demoulin, Georges Beainy, Celia Castro, Philippe Pareige, Larysa Khomenkova, et al.. Origin of Pr 3+ luminescence in hafnium silicate films: combined atom probe tomography and TEM investigations. *Nano Futures*, 2018, 2 (3), pp.2. 10.1088/2399-1984/aad009 . hal-01845624

HAL Id: hal-01845624

<https://hal.science/hal-01845624v1>

Submitted on 26 Aug 2018

HAL is a multi-disciplinary open access archive for the deposit and dissemination of scientific research documents, whether they are published or not. The documents may come from teaching and research institutions in France or abroad, or from public or private research centers.

L'archive ouverte pluridisciplinaire **HAL**, est destinée au dépôt et à la diffusion de documents scientifiques de niveau recherche, publiés ou non, émanant des établissements d'enseignement et de recherche français ou étrangers, des laboratoires publics ou privés.

Origin of Pr³⁺ luminescence in hafnium silicate films: combined atom probe tomography and TEM investigations

Rémi Demoulin¹, Georges Beainy¹, Célia Castro¹, Philippe Pareige¹, Larysa Khomenkova^{2,3} ,
Christophe Labbé², Fabrice Gourbilleau² and Etienne Talbot¹ 

¹ Normandie Univ, UNIROUEN, INSA Rouen, CNRS, Groupe de Physique des Matériaux, 76000 Rouen, France

² Normandie Univ, ENSICAEN, UNICAEN, CEA, CNRS, CIMAP, 14000 Caen, France

³ Present address: V. Lashkaryov Institute of Semiconductor Physics at the National Academy of Sciences of Ukraine, 45 Prospekt Naury, Kyiv 03028, Ukraine.

E-mail: etienne.talbot@univ-rouen.fr

Keywords: hafnium silicates, rare-earth ions, atom probe tomography, photoluminescence, phase transformation

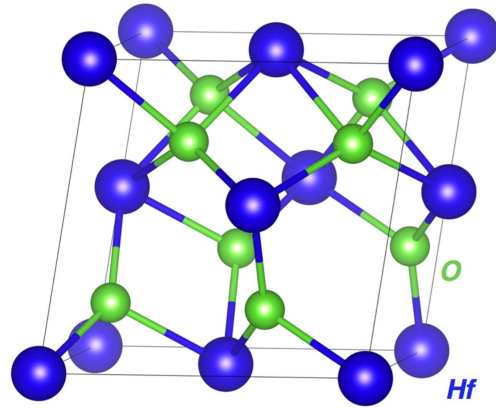
Abstract

Structural, chemical, and luminescence properties of Pr³⁺-doped HfSiO_x layers fabricated by radio-frequency magnetron sputtering were examined as a function of annealing temperature. Phase separation between SiO₂ and HfO₂ as well as the location of Pr³⁺ dopants were investigated using atom probe tomography and transmission electron microscopy while optical properties of Pr³⁺ ions were studied using photoluminescence measurements. As a result, (i) we evidenced the location of the Pr³⁺ dopants in the HfO₂ phase while the SiO₂ phase was discovered to be free of these dopants, (ii) the HfO₂ phase was identified to crystallize in the cubic phase until 1050 °C annealing, (iii) no Pr clusters were detected as function of annealing, and (iv) luminescence properties were discussed in regard to the location of Pr in the HfO₂ cubic phase.

1. Introduction

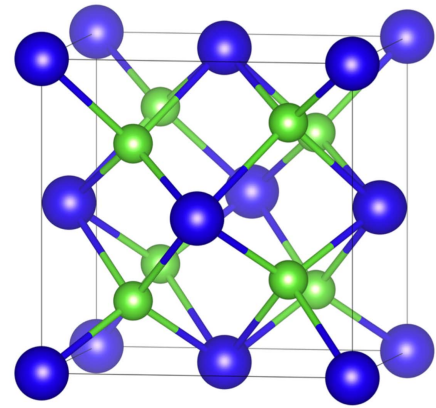
Hafnium silicates (HfSiO_x) are considered as one of the most promising highly dielectric materials to replace SiO₂ in complementary metal–oxide semiconductor technology [1]. This can be ascribed to their good thermal and chemical stabilities on Si wafer, their wide optical bandgap (5.7 eV), and their high refractive index [1–3]. Moreover, due to their lower phonon frequencies compared to SiO₂, these HfSiO_x matrices are expected to be suitable hosts for efficient activation of rare-earth (RE) optical emission. Finally, because of the large bandgap of HfSiO_x, which makes it transparent in the UV to IR range, this material is a promising host matrix for optical applications. RE ions are frequently used for light-emitting devices due to the variety of electronic levels allowing us to tune optical emission in the UV to IR range [4, 5]. Nevertheless, only a few studies have been performed on RE-doped HfSiO_x, with particular attention on Er³⁺-doped films [6–11]. The structural properties of these materials at the nanoscale level were investigated by transmission electron microscopy (TEM) [7, 9], which enabled us to reveal a phase separation between an amorphous SiO₂ and a tetragonal HfO₂ phase caused by high annealing temperature. Pure HfO₂ can exist in four crystalline phases, as presented in figure 1, depending on the conditions (temperature, pressure, etc). The most stable phase formed at normal conditions (ambient pressure and temperature lower than 1700 °C) is the monoclinic one (m-HfO₂ P2₁/c, figure 1(a)), whereas the tetragonal (t-HfO₂ P4₂/nmc, figure 1(b)) and cubic (c-HfO₂ Fm $\bar{3}$ m, figure 1(c)) phases of pure HfO₂ appear at high temperatures [12, 13]. However, the orthorhombic phase (o-HfO₂ Pca2₁, figure 1(d)) has also been observed at room temperature in Si, Al, and Gd-doped HfO₂ [14]. As can be seen from figure 1, similarity exists between the different phases. Moreover, metastable tetragonal or cubic phases can also be stabilized at room temperature by doping the HfO₂ matrix with RE atoms, as recently demonstrated for Ce-doped HfO₂ nanoparticles [10] and La-doped HfO₂ films [11]. The tetragonal HfO₂ phase was also confirmed by XRD in the Er³⁺-doped SiO₂–HfO₂ waveguide [8]. It was proposed that the introduction of RE³⁺ ions both in HfO₂ and HfSiO_x changes the coordination number of Hf⁴⁺ cations, which can be substituted by RE³⁺ ions in the lattice with a formation of vacancies in the oxygen sublattice [10, 15, 16].

a) monoclinic



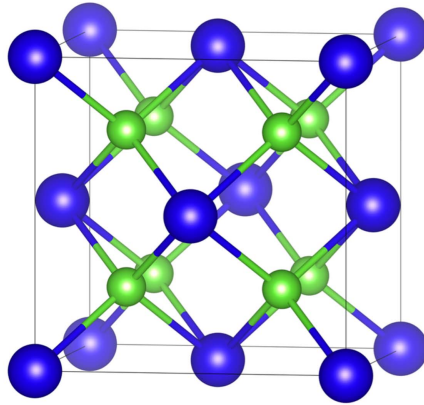
$P2_1/c$
 $a = 5.12\text{\AA}, b = 5.18\text{\AA}, c = 5.29\text{\AA}, \beta = 99.2^\circ$

b) tetragonal



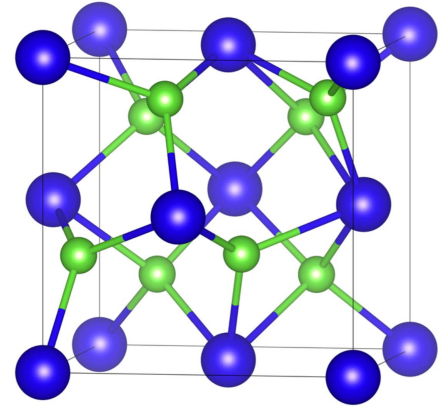
$P4_2/nmc$
 $a = 5.14\text{\AA}, c = 5.25\text{\AA}$

c) cubic



$Fm\bar{3}m$
 $a = 5.09\text{\AA}$

d) orthorhombic



$Pca2_1$
 $a = 5.04\text{\AA}, b = 5.23\text{\AA}, c = 5.06\text{\AA}$

Figure 1. Polymorph structures of (a) monoclinic, (b) tetragonal, (c) cubic, and (d) orthorhombic HfO₂ phases. Hf atoms (big) are blue, and O atoms (small) are green.

Recently, the luminescence of Pr³⁺ ions in the visible spectral range was observed in the Pr-doped HfSiO_x layer produced by magnetron sputtering [17]. A maximum of luminescence intensity was obtained for a 1000 °C annealing, and the signal was attributed to an efficient excitation by oxygen vacancies located in the HfO₂ phase. The structural properties were investigated by FTIR, XRD, and TEM, showing the phase separation between the HfO₂ and SiO₂ phases after such a high annealing temperature as well as the crystalline nature of the HfO₂ phase similar to that in Er³⁺-doped HfSiO_x films [6–9]. However, the knowledge of an accurate atomic structure of the hosting material, particularly the local environment of Pr³⁺ ions, can be important to improve and optimize Pr-based photonic devices. In this paper, we investigate the effects at the atomic scale of annealing temperature on the structure of Pr-doped HfSiO_x thin films produced by magnetron sputtering, using atom probe tomography (APT) and TEM.

2. Experimental section

2.1. Sample preparation

Pr³⁺-doped HfSiO_x was deposited on top of (100) 250 μm thick 2" Si wafers by radio-frequency magnetron co-sputtering of a pure 4" HfO₂ target (99.9% Testbourn Ltd.) topped by calibrated 1 cm² Si and Pr₆O₁₁ chips. Prior to the deposition run, the deposition chamber was maintained at a vacuum of 10⁻⁷ torr; during the run, the plasma pressure was fixed at 1.5 mTorr. Note that due to the geometry of the chamber, the substrate holder was not rotating. Before deposition, the substrates were subjected to standard RCA cleaning, dipped in a diluted 10%

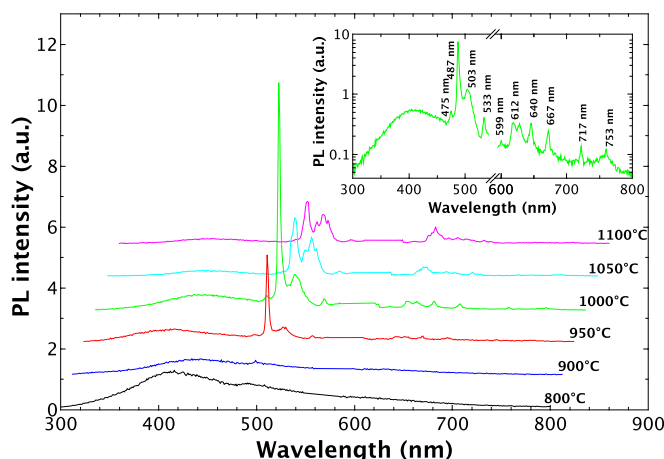


Figure 2. PL spectra of the Pr-doped HfSiO_x films annealed at different temperatures ($T_A = 800\text{ }^{\circ}\text{C}$ to $1100\text{ }^{\circ}\text{C}$). The excitation wavelength is 285 nm . Inset shows the PL spectrum in logarithmic scale for the films annealed at $T_A = 1000\text{ }^{\circ}\text{C}$.

HF solution, dried in N₂, and then transferred to the deposition chamber. The films were fabricated with a radio-frequency power density of 0.98 W cm^{-2} in a pure Ar plasma, and a substrate temperature of $25\text{ }^{\circ}\text{C}$. The optimized deposition conditions were determined on the basis of previous works done on similar Er-doped systems [6, 18]. Finally, an annealing treatment was performed under a N₂ flow at temperatures varying from $800\text{ }^{\circ}\text{C}$ up to $1050\text{ }^{\circ}\text{C}$ for 1 h.

2.2. Structural and chemical characterization

Chemical and structural analyses of the samples annealed at $800\text{ }^{\circ}\text{C}$, $950\text{ }^{\circ}\text{C}$, and $1050\text{ }^{\circ}\text{C}$ were achieved by APT using a laser-assisted wide-angle tomographic atom probe (LAWATAP-Cameca). APT is a three-dimensional (3D) high-resolution analytic microscopy that allows the spatial mapping of atoms in a sample. The APT process is based on the field evaporation of surface atoms from the tip-shaped sample with a curvature radius lower than 50 nm . Tips were prepared using a dual beam Zeiss NVision 40 FIB-SEM, by employing the lift-out and annular milling method [19]. APT experiments were conducted by applying UV femtosecond laser pulses ($\lambda = 343\text{ nm}$) with a pulse energy of 20 nJ , in an analysis chamber under a vacuum of 10^{-10} mbar . The APT data were reconstructed and analyzed using the Groupe de Physique des Matériaux's data treatment code. Cross-section TEM samples were prepared by mechanical polishing and Ar ion milling procedures. High-resolution TEM (HRTEM), selected area electron diffraction (SAED), scanning TEM (STEM), high angle annular dark field (HAADF), and electron energy loss spectroscopy (EELS) were performed on a field emission probe Cs aberration-corrected JEOL-ARM200F operating at 200 kV . EELS was performed on a GIF Quantum (Gatan) in a DUAL-EELS mode allowing us to simultaneously acquire the zero loss peak and the chosen signal. In this way any energy shift occurring during the acquisition could be corrected.

2.3. Photoluminescence (PL) measurements

PL experiments were carried out using a Jobin Yvon fluorolog spectrometer. The excitation source was a 450 W xenon arc lamp, and all spectra recorded at room temperature were corrected of the spectral response of the system.

3. Results and discussion

3.1. PL properties

The PL spectra in the UV to NIR spectral range registered for Pr-doped HfSiO_x films as a function of annealing temperature are shown in figure 2. A more detailed investigation of PL and PL excitation spectra has already been performed and can be found in [17]. PL signals of Pr³⁺ ions were observed only after annealing at $T_A \geq 950\text{ }^{\circ}\text{C}$ as sharp PL peaks associated with characteristic intra- $4f$ transitions of Pr³⁺ ions (see the inset of figure 2). For $T_A \geq 950\text{ }^{\circ}\text{C}$, the spectra show a strong luminescence intensity at 487 nm corresponding to the characteristic $^3P_0 \rightarrow ^3H_4$ transition of Pr³⁺ ions. The highest Pr³⁺ luminescence was detected for $T_A = 1000\text{ }^{\circ}\text{C}$. The increase in intensity with the annealing temperature rising from $800\text{ }^{\circ}\text{C}$ to $1000\text{ }^{\circ}\text{C}$ can be attributed to the decrease in the nonradiative recombination rates during the annealing process. At higher temperatures ($T_A > 1000\text{ }^{\circ}\text{C}$), in addition to the intensity decrease, it is interesting to observe some slight modifications in the PL

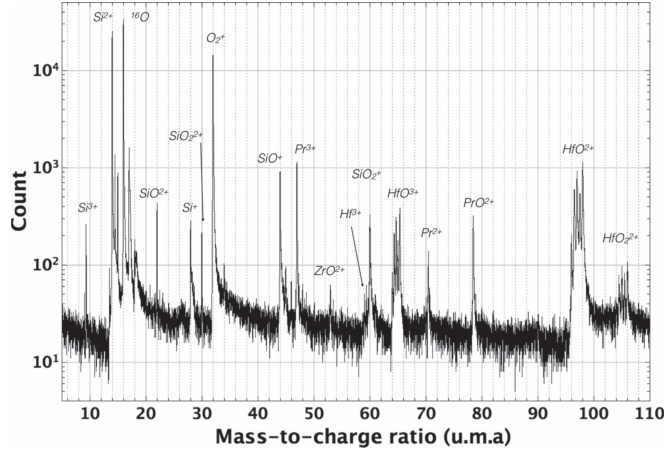


Figure 3. Mass spectrum collected by APT experiment on Pr-doped HfSiO_x film annealed at 1050 °C.

Table 1. Atomic concentration of Si, O, Hf, and Pr atoms depending on the nature of the ¹⁶O peak.

HfSiO _x :Pr@ 1050 °C	Si (at.%)	O (at.%)	Hf (at.%)	Pr (at.%)
if ¹⁶ O = O ₂ ²⁺	14.1 ± 0.3	70.6 ± 0.4	12.0 ± 0.3	3.3 ± 0.1
if ¹⁶ O = O ⁺	16.3 ± 0.3	66.1 ± 0.4	13.8 ± 0.3	3.8 ± 0.2

spectra. In fact, the position of the principal peak of emission redshifts from 487 nm at T_A = 1000 °C to 492 nm at T_A = 1100 °C. Moreover, the peak associated with the ³P₀ → ³H₄ transition at 503 nm splits into three different peaks, and the two peaks issued from the ¹D₂ → ³H₄ transition at 612 and 623 nm become one peak centered at 617 nm at 1050 °C. All of these changes in PL spectra can be caused by the structural evolution of the matrix during the annealing process and principally by a significant evolution of the environment of Pr³⁺ ions. In fact, the formation of Pr clusters as it was observed for other RE elements in a silica matrix [20, 21], or the crystallization of the HfO₂ phase in the matrix involving the modification of the crystal field near Pr³⁺ ions at high temperature, can affect the optical properties of the materials. To understand the origin of the modifications observed in the PL spectra, a thorough study of the microstructure is required.

3.2. APT results

The atom probe mass spectrum obtained for the Pr-doped HfSiO_x sample annealed at 1050 °C is shown in figure 3. All the mass peaks are well identified in term of species and charged states except the peak at 16 amu (¹⁶O). In fact, the real origin of this peak in metal–oxide matrices is still unclear; it could be identified as the evaporation of O⁺ or O₂²⁺ ions, or a mix of both. For instance, in SiO₂ matrices it was shown that O atoms were mainly evaporated in the form of O₂²⁺ [22], whereas in Fe₂O₃ metallic oxide these atoms were identified as O⁺ [23]. As a consequence, the real origin of this ¹⁶O peak seems to be strongly dependent on the nature of the metal–oxide matrix. Therefore, in the case of a bi-phased system, here composed of SiO₂ and HfO₂, the ¹⁶O peak origin can be different depending on the phase. One case of the HfSiO_x matrix has already been studied by an atom probe [24]. It was shown that the use of the O₂²⁺ form could give the compositions of the SiO₂ and HfO₂ phases that are expected in these kinds of systems. The precise nature of this peak will be discussed after HfO₂ phase identification by TEM. Concerning the other species, Si is detected as Si⁺, Si²⁺, and Si³⁺, and as molecular ions SiO⁺, SiO₂⁺, SiO²⁺, and SiO₂²⁺. Besides, we can see that Hf elements are mainly detected as molecular ions HfO²⁺, HfO³⁺, and HfO₂²⁺. Finally, Pr ions are identified as Pr²⁺, Pr³⁺, and PrO²⁺. Moreover, we detected a peak at 53.5 amu, which can be attributed to the molecular ions ZrO₂²⁺. This observation, also detected in STEM-EDS analysis (not shown here), can be explained by the presence of Zr traces in the HfO₂ target, and appeared in all analyzed samples. No Ga ions were detected, indicating that there was no Ga implantation during the FIB milling process of the tip preparation, which could damage the microstructure. The mean chemical composition of samples was computed from mass spectra by considering the two possibilities for the ¹⁶O peak, and is reported in table 1.

As we can see, the chemical nature of this peak does not significantly impact the composition of the sample. This can be explained by the large number of O atoms that are evaporated in the form of molecular ions during the experiment (figure 3). Finally, considering previous studies made on HfSiO_x by APT [24, 25], further

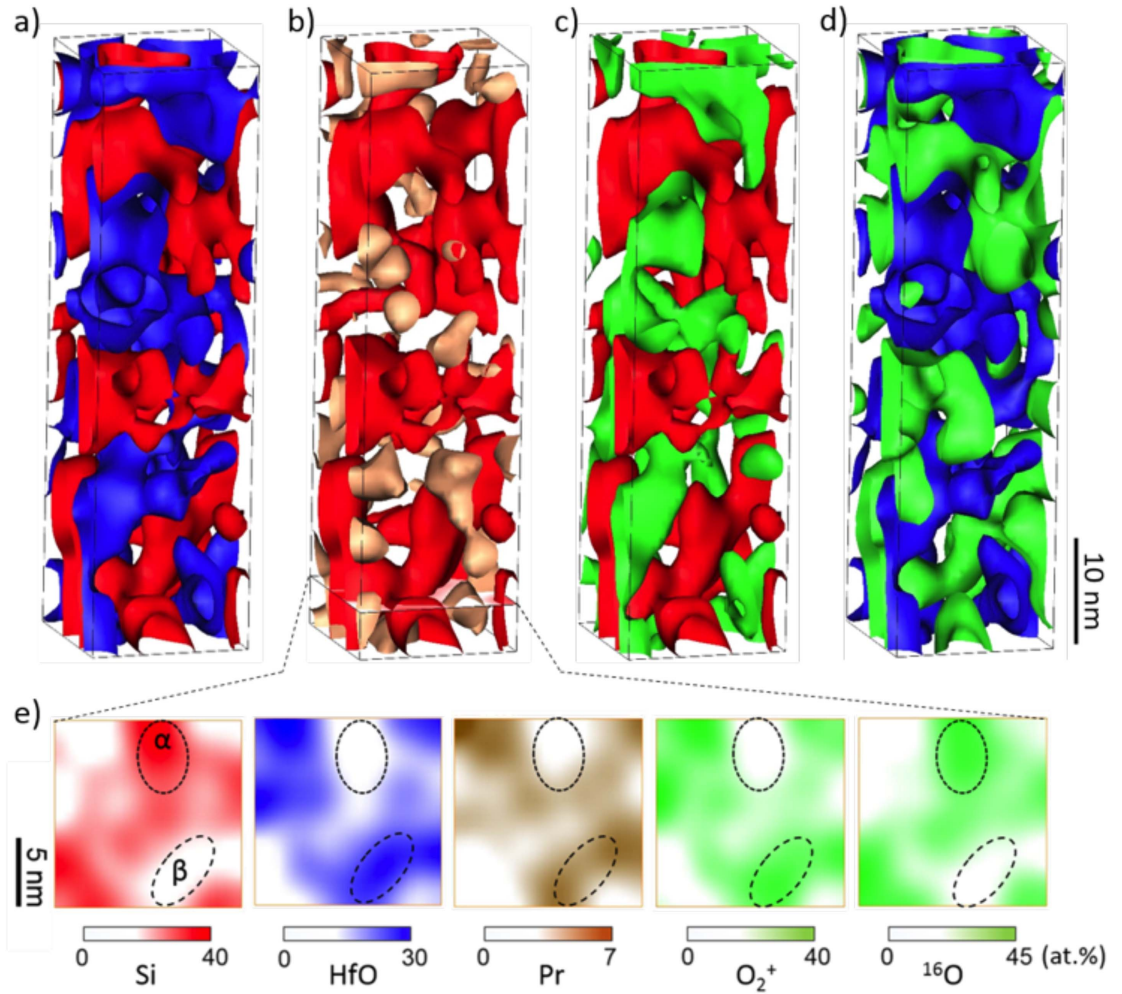


Figure 4. 3D isoconcentration surfaces for Pr-doped HfSiO_x film annealed at 1050 °C. 3D isosurfaces of (a) Si (red) and HfO (blue), (b) Si (red) and Pr (brown), (c) Si and O_2^+ (green), and (d) HfO and ^{16}O (green) concentrations are represented in a volume of $15 \times 15 \times 55 \text{ nm}^3$. Thresholds are $X_{\text{Si}} = 30 \text{ at.}\%$, $X_{\text{HfO}} = 20 \text{ at.}\%$, $X_{^{16}\text{O}} = 33 \text{ at.}\%$, $X_{\text{O}_2^+} = 27 \text{ at.}\%$, and $X_{\text{Pr}} = 2 \text{ at.}\%$. (e) Isoconcentration slices extracted from the selected region, for each map the volume is $15 \times 15 \times 0.65 \text{ nm}^3$, α and β represent Si-rich and Hf-rich phases, respectively.

calculations will take into account this ^{16}O peak as O_2^{2+} . No difference in the overall concentration has been observed as a function of the annealing temperature.

As predicted by the pseudo-binary phase diagram, and as it has been previously evidenced, a phase separation between SiO_2 and HfO_2 phases can occur in the HfSiO_x layer under annealing [25–28]. To deeply investigate this effect, the nature of phases formed, as well as the location of Pr^{3+} ions in the sample, we used APT to study the influence of annealing temperature on the structure.

The 3D isoconcentration surfaces representing the spatial distribution of Si (corresponding to Si^+ , Si^{2+} , and Si^{3+} ions), HfO (corresponding to HfO^{2+} and HfO^{3+} ions), ^{16}O , O_2^+ , and Pr (corresponding to Pr^{2+} and Pr^{3+} ions) elements in the Pr-doped HfSiO_x layer annealed at 1050 °C are shown in figures 4(a) to (d). The isoconcentration maps of Si and HfO (figure 4(a)) highlight the phase separation between Si-rich and Hf-rich phases forming two interconnected phases upon the annealing treatment. The distribution of Si and Pr (figure 4(b)) reveals that Pr atoms are located outside of the Si-rich phase. Moreover, as we can observe by investigating the isoconcentration maps of the two oxygen peaks (O_2^+ and ^{16}O) in regards to the spatial location of the Si-rich and HfO-rich phases in figures 4(c) and (d), O_2^+ ions are mainly detected outside the Si-rich phase (figure 4(c)) whereas ^{16}O are identified outside the Hf-rich phase. These results allow us to conclude that oxygen atoms were evaporated in different ways from these two different phases. This highlights a difference in the environment of O atoms between the two phases present in the system as well as a difference in the evaporation field, with a lower evaporation field required to evaporate the Hf-rich phase. Otherwise, this result confirms that the nature of the ^{16}O peak can be different according to the phase. Figure 4(e) represents the isoconcentration maps performed on a slice in the previous 3D volume. It shows the distribution of Si, HfO, Pr, ^{16}O , and O_2^+ in the Pr-doped HfSiO_x layer annealed at 1050 °C. All these elements are nonhomogeneously distributed in the

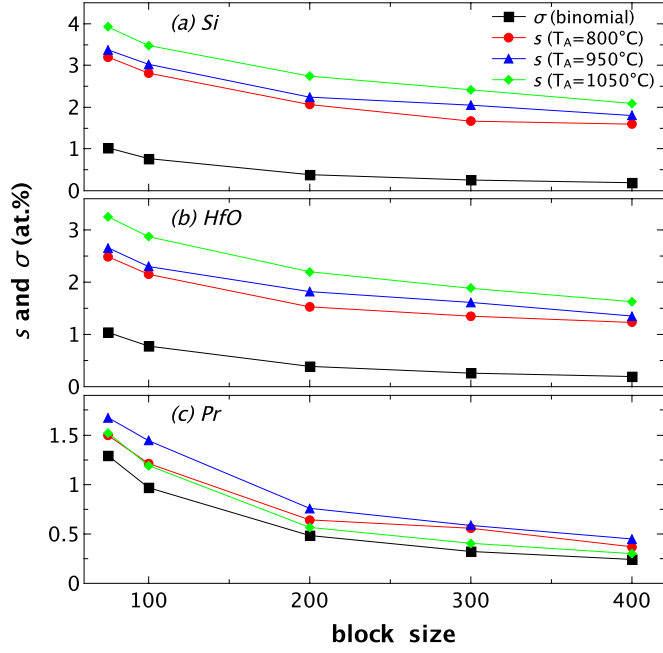


Figure 5. Statistical tests of randomness of (a) Si ions, (b) HfO ions, and (c) Pr ions distributions in Pr-doped HfSiO_x films annealed at 800 °C, 950 °C, and 1050 °C.

analyzed volume, as displayed in figures 4(a)–(d). As shown in figure 4(a), two regions can be clearly identified corresponding to Si-rich and Hf-rich phases, respectively named α and β in figure 4(e). The presence of these two phases is governed by the HfSiO_x decomposition upon annealing, which should be finalized by the formation of SiO₂ and HfO₂ as proved by several studies [25–29]. Besides, it has been evidenced that the decomposition of the HfSiO_x layers occurs in the form of a spinodal decomposition [28, 30], which is consistent with the 3D isoconcentration surfaces observed in figure 4(a). Moreover, regarding the distribution of Pr elements in the volume (figure 4(e)), these atoms clearly appear to be located in Hf-rich phases. A similar behavior of RE dopant atoms has already been mentioned in the case of Er-doped SiO₂–HfO₂ [7], which explained that Er atoms can diffuse into HfO₂ nanocrystals after heat treatment, leading to an improvement of the luminescence signal. The same maps were investigated on Pr-doped HfSiO_x layers annealed at 800 °C and 950 °C (not shown here), but these maps did not reveal a significant evolution of the phase decomposition or of a change in dopant location during the annealing process.

In order to confirm and quantify the nonhomogeneous distribution of atoms in the volume upon annealing, statistical tests of randomness described by Thuvander *et al* [31] were performed to observe the evolution of the atomic distribution upon sample annealing. Results of these tests for the distribution of Si, HfO, and Pr ions in the layers annealed at 800 °C, 950 °C, and 1050 °C are presented in figures 5(a), (b), and (c), respectively. The goal of the statistical test of randomness is to compare the standard error (s) of the frequency distribution of an element (Si, HfO, and Pr) extracted from APT reconstruction to the standard deviation (σ) of the binomial distribution (case of randomness distribution). In the case of a homogeneous (random) distribution of elements in the material, both s and σ curves must be superimposed. All graphs represented in figure 5 show that s and σ curves are not superimposed, and confirm that these three elements, Si, HfO, and Pr, are nonhomogeneously distributed in the analyzed volume; however, their evolution according to annealing seems to be different. In fact, for Si and HfO distributions, we can notice an up-shift of the s -curve while the temperature increases from 800 °C to 1050 °C (figures 5(a), (b)). As a result, the distribution of ions is more homogeneous at the lower annealing temperature. This reveals an evolution of the matrix during the annealing treatment from 800 °C to 1050 °C, which should correspond to a progressive phase separation between SiO₂ and HfO₂ phases observed in HfSiO_x. In the case of Pr atoms (figure 5(c)), we can first observe an up-shift for the s -curve when the annealing temperature rises from 800 °C to 950 °C, and then see a down-shift of the s -curve when the temperature increases from 950 °C to 1050 °C. The first step can be explained by considering the demixing of Si-rich and HfO-rich zones and the formation of a Pr-rich area (located in Hf-rich phases, as evidenced previously in figure 4). The second stage can be ascribed to a redistribution of Pr atoms located in the Hf-rich phases. This result reveals a modification of Pr³⁺ ions' environment between the samples annealed at 950 °C and 1050 °C, which could induce a change in the optical activities of these ions as was observed in the PL spectra shown in figure 2(a). Up to now, no Pr clusters have been evidenced in the matrix. Consequently, the change of Pr³⁺ ion

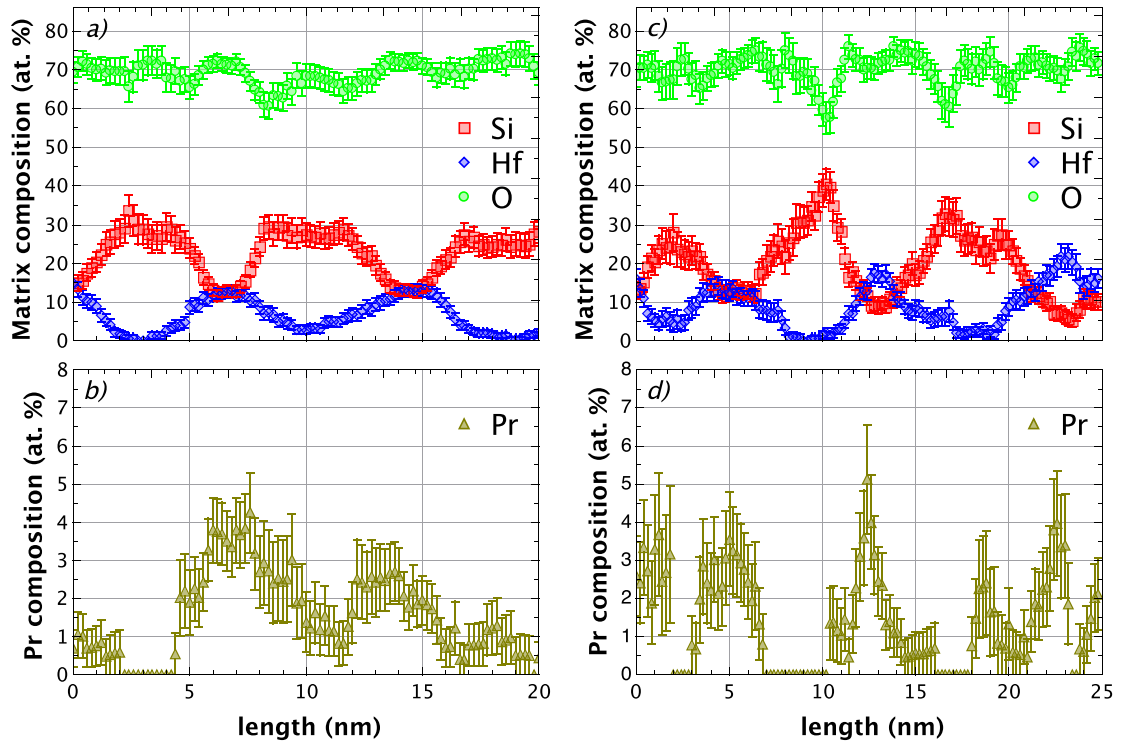


Figure 6. Composition profile computed on Pr-doped HfSiO_x annealed at (a), (b) 950 °C, and (c), (d) 1050 °C. (a), (c) Matrix composition (Si, Hf, and O) and (b), (d) Pr composition. The sample volumes are, respectively, (a), (b) $2 \times 2 \times 20 \text{ nm}^3$ and (c), (d) $2 \times 2 \times 25 \text{ nm}^3$.

emission should be due to an evolution of the microstructure of the Hf-rich phase and the environment of Pr^{3+} ions.

In order to define the microstructure of these materials accurately, it can be helpful to focus on the composition of each phase. The composition profiles in the analyzed volumes were computed in the films annealed at 950 °C and 1050 °C, and are presented in figures 6(a), (b), (c), and (d) respectively. As mentioned above, the composition of Si and Hf vary along the length according to the phase separation of Si-rich and HfO-rich phases. The concentration of Pr atoms reaches a maximum of 4 at.% in the Hf-rich phase, and is almost zero in the Si-rich phase. Moreover, the distance between the cores of each type of phase (wavelength of the decomposition) varies from 8 to 10 nm for both samples. The mean chemical composition of Si-rich and Hf-rich zones was determined by placing small boxes of $2 \times 2 \times 2 \text{ nm}^3$ in the core of each zone in the entire volume. By counting the number of atoms of each species present in the boxes, a mean value of the composition of Si-rich and Hf-rich phases can be computed. The mean composition of Si-rich phase for the samples annealed at 950 °C and 1050 °C are, respectively, $X_{\text{Si}} = 31.3 \pm 3.2 \text{ at.}\%$ and $X_{\text{O}} = 68.7 \pm 3.2 \text{ at.}\%$, and $X_{\text{Si}} = 29.9 \pm 3.0 \text{ at.}\%$ and $X_{\text{O}} = 70.1 \pm 3.0 \text{ at.}\%$; this can be attributed unambiguously to the SiO_2 phase. Regarding the Hf-rich phase, we can observe in figures 6(a) and (c) 7 to 11 at.% of Si is counted in these zones. This suggests that the phase separation between SiO_2 and HfO_2 is still in progress. In fact, pseudo-binary phase diagrams of the SiO_2 – HfO_2 system [32, 33] highlights the existence of a third compound, HfSiO_4 . Then, depending on the mole fraction of SiO_2 and HfO_2 , the phase separation from HfSiO_x to $x.\text{SiO}_2 + (1 - x).\text{HfO}_2$ is realized, passing through an intermediate stage composed of SiO_2 and HfSiO_4 or HfO_2 and HfSiO_4 . However, at this temperature ($T \sim 1000 \text{ °C}$), the separation between the two phases should be in an advanced state. In this case, the presence of Si atoms is unexpected in the Hf-phase and could be considered as an artifact of the APT analysis. Since a difference in evaporation field exists between silica and hafnia, the composition measurements of a such complex nanometric structure (figure 4(a)) can be altered because of the well-known effect of local magnification [34] that can occur in bi-phased systems. Otherwise, this effect was previously evidenced in similar material [24, 25]. The raw and corrected (from the local magnification effect) mean compositions of Hf-rich phases was computed in the samples annealed at 950 °C and 1050 °C. Results are reported in table 2. There was no significant evolution of the composition of Hf-rich phases between these two samples. In each case, the nature of the Hf-rich phase could not directly be attributed to HfSiO_4 nor HfO_2 . Finally, none of these results allowed us to extract with accuracy the stoichiometry of the Hf-rich phase from APT analysis, but they confirmed the favored location of Pr atoms in this Hf-rich phase.

Table 2. Mean atomic concentration of Si, O, Hf, and Pr atoms in Hf-rich phases.

HfSiO _x :Pr	Si (at.%)	O (at.%)	Hf (at.%)	Pr (at.%)
950 °C	9.0 ± 1.1	71.5 ± 1.7	15.6 ± 1.3	3.9 ± 0.7
1050 °C	7.9 ± 1.1	73.5 ± 1.6	16.1 ± 1.4	2.5 ± 0.6
Correction of local magnification effect				
950 °C	0	73.2 ± 1.9	21.4 ± 1.8	5.4 ± 1.0
1050 °C	0	75.7 ± 1.8	21.1 ± 1.7	3.2 ± 0.7

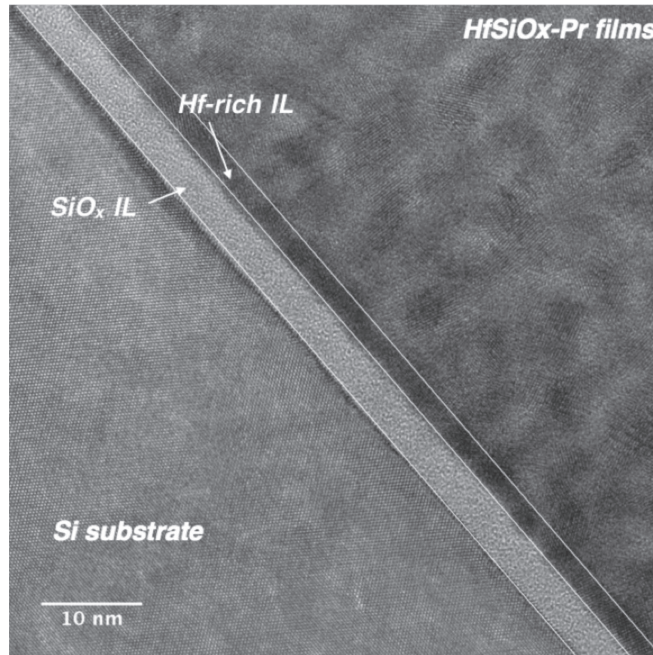


Figure 7. Cross sectional HRTEM micrograph of the HfSiO_x-Pr sample annealed at 1050 °C oriented according the [011] zone axis of the Si substrate. SiO_x IL denotes the thin (~4 nm) SiO₂ layer at the interface with the Si substrate. Hf-rich IL denotes the Hf-rich IL following the SiO_x IL.

3.3. SAED and HRTEM results

In order to elucidate the nature of the Hf-rich phase and to confirm the location of Pr³⁺ ions, we performed TEM analysis on the HfSiO_x-Pr samples annealed at 950 °C and 1050 °C. Figure 7 shows a cross sectional HRTEM image of the HfSiO_x-Pr sample annealed at 1050 °C. The micrograph shows a nanocrystalline structure in this film and the formation of two interfacial layers (ILs). The observed dark and bright regions can be explained by the phase separation between Si-rich and Hf-rich phases already evidenced in the APT experiments (figure 4). The Hf-rich phase is clearly crystallized. These observations are consistent with previous investigations on phase separation of the HfSiO_x matrix, and were predicted by a phase diagram [24, 26, 32]. Based on the observed contrast, we can expect that the first IL (bright region, SiO_x-IL), with a thickness of 4 nm, contains no or very little Hf, and deals with SiO_x or SiO₂. The second one seems more concentrated in Hf atoms (Hf-rich IL of about ~3 nm). Similar IL formation has already been evidenced and identified by TEM and APT experiments on HfSiO_x grown by magnetron sputtering [24]. The sample annealed at 950 °C presents a similar micrograph (not shown here).

The nature of the crystalline phase present in samples annealed at 950 °C and 1050 °C was examined from SAED patterns (figures 8(a) and (b)). For both annealed samples, the four main diffraction rings of the SAED pattern can be indexed with the cubic fluorite type structure of HfO₂ (space group *Fm* $\bar{3}$ *m*). The d_{hkl} spacing extracted from these SAED are 2.89 Å, 2.51 Å, 1.76 Å, and 1.49 Å for the 950 °C annealed sample, and 2.85 Å, 2.50 Å, 1.75 Å, and 1.48 Å for the 1050 °C annealed sample. In both cases, the d_{hkl} spacings can be assigned to the (111), (200), (220), and (311) lattice planes of the cubic HfO₂ phase (PDF 00-053-0550). No significant crystallographic phase transition is observed with the annealing treatment between 950 °C and 1050 °C. This result is also demonstrated by previous XRD experiments where HfO₂ phases were wrongly determined to be

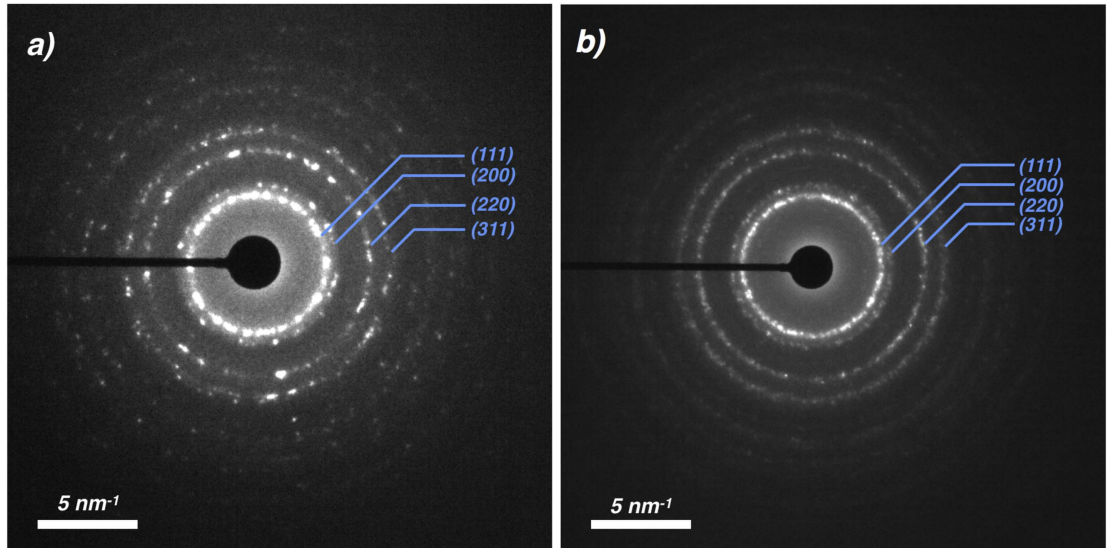


Figure 8. SAED pattern of HfSiO_x-Pr samples annealed at (a) 950 °C and (b) 1050 °C.

tetragonal [17]. It should be noted that an ambiguity can exist in indexing the HfO₂ XRD pattern where tetragonal and cubic phases can present a very similar pattern. As mentioned previously, RE-doped HfO₂ can present a cubic crystallographic phase. Based on the results described above, we can assume that this mechanism is similar in Pr-doped HfSiO_x films where (i) spinodal decomposition leads to the formation of HfO₂-rich and SiO₂-rich nanocrystalline phases and (ii) Pr³⁺ ions stabilize the cubic phase of the HfO₂ for an annealing temperature between 950 °C and 1050 °C. Previous XRD and SAED experiments on the 1100 °C sample have shown that an increase in annealing temperature can induce a phase transformation to the monoclinic phase [17].

SAED and HRTEM experiments allow us to conclude that the Hf-rich phase identified with APT deals with HfO₂ and that the Si atoms detected inside the Hf-rich phase (figure 6) are only due to the local magnification artifact occurring during APT experiments. It should be noted that the observed phases after decomposition (SiO₂ and HfO₂) do not deal with those predicted by the HfO₂-SiO₂ phase diagram (HfO₂+HfSiO₄ or SiO₂+HfSiO₄) or with the thermodynamic computation of a ternary Hf-Si-O diagram [32]. Moreover, no sign of the formation of Pr silicates (mainly Pr₂Si₂O₇) has been observed.

3.4. HAADF-STEM and EELS study

The phase separation in Hf-rich and Si-rich interconnected structures occurring with annealing was confirmed by a combined HAADF-STEM and EELS experiments. The HAADF image, sensitive to the Z-contrast, of the 950 °C annealed sample is presented in figure 9(a). The micrograph exhibits high-Z (bright) and low-Z (dark) regions, which can be attributed to HfO₂-rich (bright) and SiO₂-rich (dark) phases. This result was confirmed by an EELS line scan profile performed over bright and dark areas from point A to point B (figure 9(a)). Figures 9(b) and (d) present the EELS line scan and extracted EELS spectra in the SiO₂-rich and HfO₂-rich phases in the O-K edge region. Both contrasted zones contain oxygen with a characteristic signal of an O-K edge around 540 eV. Moreover, we note a low energy loss shift of the O-K edge in the bright region (for depths between 2–5 nm, 9–13 nm, and 17–22 nm (figure 9(d))), which confirms the chemical difference between dark and bright regions. Such a shift has already been evidenced between SiO₂ and HfO₂ phases [24, 35]. The Pr-M_{4,5} EELS spectrum is depicted in figure 9(c), and a typical EELS spectrum (extracted from HfO₂-rich regions in figure 9(c)) is presented in figure 9(e). The Pr EELS signal, characterized by the typical two M₅ and M₄ white lines, is only present in the bright region (i.e. the HfO₂-rich region). Moreover, the M₅ and M₄ peaks are located at 932 eV and 951 eV, which is in agreement with the EELS signal of Pr ions [36]. The intensity ratio between M₅ and M₄ lines, which is directly related to the number of electrons in the *f* shell, is measured to be $I_{M_5}/I_{M_4} \sim 1.4$. This ratio is a direct signature of the presence of Pr³⁺ ions as well as the damping of shoulders at the lower energy side of the M₄ peak. In the case of Pr in the 4+ valence state, the intensity ratio should be close to unity and damping of the shoulder should occur at the higher energy side of the M₅ peak [36–38]. This result allows us to conclude unambiguously that Pr ions are preferentially located in the HfO₂-rich region, as already evidenced in the APT results and in the form of Pr³⁺.

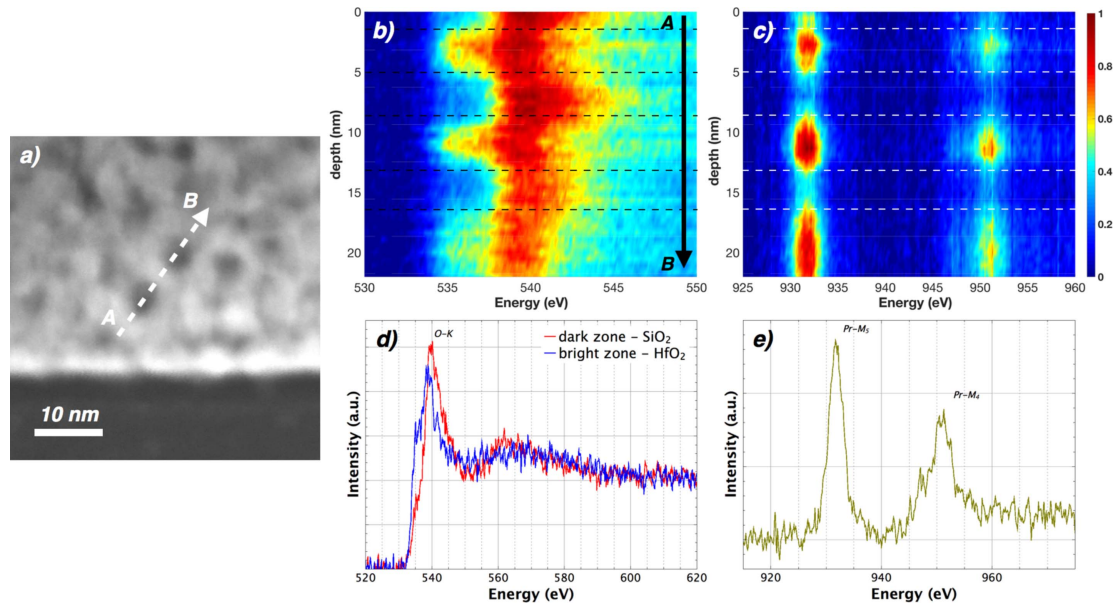


Figure 9. (a) HAADF-STEM image of cross-section lamellae in Pr-doped HfSiO_x films annealed at 950 °C. EELS spectrum 2D image from a line scan (indicated by an arrow in (a)) of (b) the O–K edge and (c) the Pr–M₄ and Pr–M₅ edges. EELS spectra extracted from Si-rich and Hf-rich zones for (d) the O–K edge and (e) the Pr–M_{4,5} edge.

3.5. Discussion

Numerous studies on undoped HfSiO_x systems have shown that the structural evolution of HfSiO_x thin layers under annealing is strongly dependent on the initial composition of the layer, but all of them agree that the phase decomposition occurring in these HfSiO_x layers should end on a bi-phased system composed of an amorphous SiO₂ phase and crystalline HfO₂ phase [24, 26–29]. Moreover, it has been shown by APT experiments that Si nanocrystals can grow in Si-rich HfSiO_x thin films [24, 25]. Here, the Pr³⁺ doping of the HfSiO_x thin layers does not seem to affect the phase separation mechanism compared to the undoped HfSiO_x system. APT analyses and TEM experiments have shown the phase separation, which began at 800 °C (figure 5), between Si-rich and Hf-rich phases; these results are attributed to SiO₂-rich and HfO₂-rich phases, respectively. Contrary to the RE³⁺ doping of SiO_x matrices for which a precipitation of RE ions in the form of clusters was evidenced in the case of Er³⁺ and Ce³⁺ doping by the formation of RE silicates [20, 39], the presence of Pr³⁺ ions in the matrix does not lead to the formation of Pr oxides or Pr silicates during the annealing process at high temperature. We observed that Pr³⁺ ions tend to diffuse into the HfO₂-rich phase from the beginning of the phase decomposition, and are already present in the HfO₂-rich phase at 800 °C. At higher annealing temperatures (950 °C and 1050 °C), there is no significant evolution in the structure of the matrix in 3D mapping, and Pr³⁺ ions remain located in the HfO₂-rich phase (figures 4 and 9). However, statistical testing (figure 5) revealed a more homogeneous distribution of Pr³⁺ in the host matrix after a 1050 °C annealing treatment than after 950 °C annealing. This redistribution of Pr³⁺ in the HfO₂-rich phase can be explained by a local modification of the Pr³⁺ environment provided by the crystallization of the HfO₂-rich phase at high temperature. The presence of a crystalline form of HfO₂ in HfSiO_x-Pr thin layers has been evidenced via SAED patterns and TEM experiments (figures 7 and 8), and has been attributed to the cubic fluorite type structure of HfO₂ of space group *Fm* $\bar{3}$ *m*. This crystalline phase appeared only for annealing temperatures higher than 950 °C. The thin film of HfO₂ usually crystallizes in the monoclinic form, which is the most stable structure of the HfO₂ crystallized state at low temperatures (around 500 °C) [40, 41]. Several studies on RE-doped HfO₂ have made similar observations by highlighting the stabilization of the cubic HfO₂ phase [10, 11, 15, 42, 43]; this was observed here with SAED patterns (figure 8). The incorporation of RE dopants that have an ionic radius larger than that of Hf⁴⁺ cations tends to stabilize the cubic form of HfO₂. According to the literature, the sevenfold coordination of Hf⁴⁺ cations is favored in the monoclinic structure [41]. However, the incorporation of RE³⁺ ions in the crystal lattice changes the coordination number of Hf⁴⁺ cations from sevenfold to eightfold, and leads to the stabilization of the cubic HfO₂ form. Moreover, the Hf⁴⁺ cations can be substituted by RE³⁺ ions in the lattice; this substitution is followed by the formation of oxygen vacancies in order to maintain the electroneutrality of the crystal lattice and help stabilize the cubic crystalline phase [15]. The presence of these oxygen vacancies in the host matrix can introduce some defect states in the bandgap of HfO₂ [44, 45], which leads to the formation of recombination centers required for the excitation of electron–hole pairs. Pr³⁺ ions do not present an absorption band around 285 nm, and consequently, the direct excitation of Pr³⁺ ions is not allowed with the 285 nm wavelength used to

establish PL spectra (figure 2). This confirms the presence of an efficient energy transfer between Pr^{3+} ions and the host matrix. Considering that Pr^{3+} ions are mainly located in the cubic HfO_2 phase, as proved by APT experiments (figure 4(e)) and confirmed by the EELS spectrum (figure 9(c)), and due to the overlapping of created defect states and absorption levels of Pr^{3+} ions, excitons can transfer their energy to Pr^{3+} ions and improve the PL emission. In this way, the enhancement of PL intensity observed from $T_A = 950^\circ\text{C}$ to $T_A = 1000^\circ\text{C}$, can be explained by the growth and stabilization of the cubic HfO_2 phase providing more oxygen vacancies in that HfO_2 crystalline phase. At a higher temperature some new diffraction peaks appear on XRD spectra [17], revealing the development of a monoclinic HfO_2 phase. The cubic to monoclinic transformation could occur in an optically inactive configuration of Pr^{3+} ions, thus leading to the quenching of PL emission.

4. Conclusion

The structure of $\text{HfSiO}_x\text{-Pr}$ thin layers elaborated by magnetron sputtering was investigated by APT and TEM experiments. The phase separation between SiO_2 and HfO_2 has been highlighted for $T_A \geq 800^\circ\text{C}$. The introduction of Pr^{3+} in HfSiO_x does not lead to the formation of Pr clusters in the host matrix even at high temperature. However, Pr^{3+} ions tend to diffuse in the HfO_2 phase from the beginning of the phase separation. At high temperature, during the crystallization of the HfO_2 phase, the substitution of Hf^{4+} by Pr^{3+} leads to stabilization of the cubic crystalline form of HfO_2 and allows the formation of oxygen vacancies to ensure the electroneutrality of the crystal lattice. These oxygen vacancies, seen as defect states in the bandgap of HfO_2 , are efficient sensitizers for the excitation of Pr^{3+} ions, and permit the energy transfer between Pr^{3+} ions and the cubic HfO_2 phase.

Acknowledgments

G Beany acknowledges financial support from the Région Haute-Normandie.

ORCID iDs

Larysa Khomenkova  <https://orcid.org/0000-0002-5267-5945>

Etienne Talbot  <https://orcid.org/0000-0001-6389-1670>

References

- [1] Choi J H, Mao Y and Chang J P 2011 Development of hafnium based high- κ materials—a review *Mater. Sci. Eng., R* **72** 97–136
- [2] He G, Zhu L, Sun Z, Wan Q and Zhang L 2011 Integrations and challenges of novel high- κ gate stacks in advanced CMOS technology *Prog. Mater. Sci.* **56** 475–572
- [3] Wilk G D, Wallace R M and Anthony J M 2001 High- κ gate dielectrics: current status and materials properties considerations *J. Appl. Phys.* **89** 5243
- [4] Fujii M, Yoshida M, Kanzawa Y, Hayashi S and Yamamoto K 1997 1.54 μm photoluminescence of Er^{3+} doped into SiO_2 films containing Si nanocrystals: evidence for energy transfer from Si nanocrystals *Appl. Phys. Lett.* **71** 1198–200
- [5] Li J, Zalloum O H Y, Roschuk T, Heng C L, Wojcik J and Mascher P 2008 Light emission from rare-earth doped silicon nanostructures *Adv. Opt. Technol.* **2008** 295601
- [6] Khomenkova L, An Y-T, Khomenkov D, Portier X, Labbé C and Gourbilleau F 2014 Spectroscopic and structural investigation of undoped and Er^{3+} doped hafnium silicate layers *Phys. B* **453** 100–6
- [7] Righini G C *et al* 2009 Er^{3+} -doped silica-hafnia films for optical waveguides and spherical resonators *J. Non. Cryst. Solids* **355** 1853–60
- [8] Minati L, Speranza G, Micheli V, Ferrari M and Jestin Y 2009 X-ray photoelectron spectroscopy of Er^{3+} -activated $\text{SiO}_2\text{-HfO}_2$ glass-ceramic waveguides *J. Phys. D: Appl. Phys.* **42** 15408
- [9] Jestin Y *et al* 2007 Erbium activated HfO_2 based glass-ceramics waveguides for photonics *J. Non. Cryst. Solids* **353** 494–7
- [10] Gálvez-Barboza S, González L A, Puente-Urbina B A, Saucedo-Salazar E M and García-Cerda L A 2015 Preparation and characterization of Ce-doped HfO_2 nanoparticles *J. Alloys Compd.* **643** S62–6
- [11] Smirnova T P, Yakovkina L V and Borisov V O 2015 Impact of lanthanum on the modification of HfO_2 films structure *J. Rare Earths* **33** 857–62
- [12] Wang J, Li H P and Stevens R 1992 Hafnia and hafnia-toughened ceramics *J. Mater. Sci.* **27** 5397–430
- [13] Tang J, Zhang F, Zoogman P, Fabbri J, Chan S-W, Zhu Y, Brus L E and Steigerwald M L 2005 Martensitic phase transformation of isolated HfO_2 , ZrO_2 , and $\text{Hf}_x\text{Zr}_{1-x}\text{O}_2$ ($0 < x < 1$) nanocrystals *Adv. Funct. Mater.* **15** 1595–602
- [14] Park M H, Schenk T, Fancher C M, Grimley E D, Zhou C, Richter C, LeBeau J M, Jones J L, Mikolajick T and Schroeder U 2017 A comprehensive study on the structural evolution of HfO_2 thin films doped with various dopants *J. Mater. Chem. C* **5** 4677–90
- [15] Matović B, Bučevac D, Prekajski M, Maksimović V, Gautam D, Yoshida K and Yano T 2012 Synthesis and characterization of nanometric yttrium-doped hafnia solid solutions *J. Eur. Ceram. Soc.* **32** 1971–6
- [16] Yong-Qiang M, Zheng-Tang L, Li-Ping F and Shuai C 2014 Influence of rapid thermal annealing on the structure and electrical properties of Ce-doped HfO_2 gate dielectric *Chin. Phys. Lett.* **31** 77702
- [17] An Y T, Labbé C, Khomenkova L, Morales M, Portier X and Gourbilleau F 2013 Microstructure and optical properties of Pr^{3+} -doped hafnium silicate films *Nanoscale Res. Lett.* **8** 43

- [18] Khomenkova L, An Y-T, Labbé C, Portier X and Gourbilleau F 2012 Hafnia-based luminescent insulator for phosphor applications *ECS Trans.* **45** 1119–128
- [19] Thompson G B, Miller M K and Fraser H L 2004 Some aspects of atom probe specimen preparation and analysis of thin film materials *Ultramicroscopy* **100** 25–34
- [20] Talbot E, Lardé R, Pareige P, Khomenkova L, Hijazi K and Gourbilleau F 2013 Nanoscale evidence of erbium clustering in Er-doped silicon-rich silica *Nanoscale Res. Lett.* **8** 39
- [21] Debieu O, Bréard D, Podhorodecki A, Zatoryb G, Misiewicz J, Labbé C, Cardin J and Gourbilleau F 2010 Effect of annealing and Nd concentration on the photoluminescence of Nd³⁺ ions coupled with silicon nanoparticles *J. Appl. Phys.* **108** 113114
- [22] Roussel M, Talbot E, Pareige P and Gourbilleau F 2013 Influence of the supersaturation on Si diffusion and growth of Si nanoparticles in silicon-rich silica *J. Appl. Phys.* **113** 063519
- [23] Bachhav M, Danoix F, Hannover B, Bassat J M and Danoix R 2013 Investigation of O-18 enriched hematite (α -Fe₂O₃) by laser assisted atom probe tomography *Int. J. Mass Spectrom.* **335** 57–60
- [24] Talbot E, Roussel M, Genevois C, Pareige P, Khomenkova L, Portier X and Gourbilleau F 2012 Atomic scale observation of phase separation and formation of silicon clusters in Hf high- κ silicates *J. Appl. Phys.* **111** 103519
- [25] Talbot E, Roussel M, Khomenkova L, Gourbilleau F and Pareige P 2012 Atomic scale microstructures of high- κ HfSiO thin films fabricated by magnetron sputtering *Mater. Sci. Eng. B* **177** 717–20
- [26] Khomenkova L, Dufour C, Coulon P-E, Bonafos C and Gourbilleau F 2010 High- κ Hf-based layers grown by RF magnetron sputtering *Nanotechnology* **21** 095704
- [27] Stemmer S, Li Y, Foran B, Lysaght P S, Streiffer S K, Fuoss P and Seifert S 2003 Grazing-incidence small angle x-ray scattering studies of phase separation in hafnium silicate films *Appl. Phys. Lett.* **83** 3141–3
- [28] Kim H and McIntyre P C 2002 Spinodal decomposition in amorphous metal–silicate thin films: phase diagram analysis and interface effects on kinetics *J. Appl. Phys.* **92** 5094
- [29] Lucovsky G, Rayner G B, Kang D, Hinkle C L and Hong J G 2004 A spectroscopic study distinguishing between chemical phase separation with different degrees of crystallinity in Zr(Hf) silicate alloys *Surf. Sci.* **566-568** 772–6
- [30] Lysaght P, Foran B, Stemmer S, Bersuker G, Bennett J, Tichy R, Larson L and Huff H R 2003 Thermal response of MOCVD hafnium silicate *Microelectron. Eng.* **69** 182–9
- [31] Thuvander M, Andrén H-O, Stiller K and Hu Q-H 1998 A statistical method to detect ordering and phase separation by APFIM *Ultramicroscopy* **73** 279–85
- [32] Shin D, Arróyave R and Liu Z-K 2006 Thermodynamic modeling of the Hf-Si-O system *Calphad* **30** 375–86
- [33] Maria J-P, Wickaksana D, Parrette J and Kingon A I 2002 Crystallization in SiO₂–metal oxide alloys *J. Mater. Res.* **17** 1571–9
- [34] Vurpillot F, Bostel A and Blavette D 2000 Trajectory overlaps and local magnification in three-dimensional atom probe *Appl. Phys. Lett.* **76** 3127–9
- [35] Agustin M P, Bersuker G, Foran B, Boatner L A and Stemmer S 2006 Scanning transmission electron microscopy investigations of interfacial layers in HfO₂ gate stacks *J. Appl. Phys.* **100** 024103
- [36] Lopez-Cartes C, Bernal S, Calvino J J, Cauqui M A, Blanco G, Perez-Omil J A, Pintado J M, Helveg S and Hansen P L 2003 *In situ* transmission electron microscopy investigation of Ce(IV) and Pr(IV) reducibility in a Rh (1%)/Ce_{0.8}Pr_{0.2}O_{2-x} catalyst *Chem. Commun.* **0** 644–5
- [37] Manoubi T, Colliex C and Rez P 1990 Quantitative electron energy loss spectroscopy on M45 edges in rare earth oxides *J. Electron Spectrosc. Relat. Phenom.* **50** 1–18
- [38] Thole B T, van der Laan G, Fuggle J C, Sawatzky G A, Karnatak R C and Esteva J-M 1985 3d x-ray-absorption lines and the 3d⁹4fⁿ⁺¹ multiplets of the lanthanides *Phys. Rev. B* **32** 5107–18
- [39] Beainy G, Weimmerskirch-Aubatin J, Stoffel M, Vergnat M, Rinnert H, Pareige P and Talbot E 2017 Correlation between the nanoscale structure and the optical properties of Ce-doped SiO_{1.5} thin films *J. Lumin.* **191** 88–91
- [40] Nishide T, Honda S, Matsuura M and Ide M 2000 Surface, structural and optical properties of sol-gel derived HfO₂ films *Thin Solid Films* **371** 61–5
- [41] Štefanić G and Musić S 2001 Thermal behavior of the amorphous precursors of the HfO₂-Fe₂O₃ system *Thermochim. Acta* **373** 59–67
- [42] Mendoza-Mendoza E, Quintero-García J S, Puente-Urbina B A, Rodríguez-Fernández O S and García-Cerda L A 2017 Synthesis and characterization of Ce-doped HfO₂ nanoparticles in molten chlorides *J. Alloys Compd.* **692** 448–53
- [43] Chen S, Liu Z, Feng L, Che X and Zhao X 2014 Effect of ytterbium inclusion in hafnium oxide on the structural and electrical properties of the high- κ gate dielectric *J. Rare Earths* **32** 580–4
- [44] Xiong K, Du Y, Tse K and Robertson J 2007 Defect states in the high-dielectric-constant gate oxide HfSiO₄ *J. Appl. Phys.* **101** 024101
- [45] Kumar S, Rai S B and Rath C 2018 Monoclinic to cubic phase transformation and photoluminescence properties in Hf_{1-x}Sm_xO₂ (x = 0 – 0.12) nanoparticles *J. Appl. Phys.* **123** 55108